

Spin Hall effect and Zitterbewegung in a quasi-one-dimensional electron waveguide

P. Brusheim* and H. Q. Xu†

Division of Solid State Physics, Lund University, Box 118, S-22100 Lund, Sweden.

(Dated: February 8, 2020)

We study spin resolved probability distributions for electrons in a quasi-one-dimensional waveguide. For a spin-unpolarized injected electron beam, spin accumulation along the edges of a wide waveguide is found as well as internal patterns with alternating spin-polarization direction formed inside the waveguide. It is found that the structure of the pattern is directly related to the number of conducting channels in the leads. The calculated probability distributions reveals a reversal of the spin Hall effect in the lowest lying channels. We deduce that the SOI induced Zitterbewegung and the intrinsic spin-Hall effect are essentially the same thing and only differ in the injection and measuring conditions.

PACS numbers:

Spin-orbital interaction (SOI) is a relativistic effects: it arises from the fact that an electron moving with a finite momentum in a non-uniform potential will see an effective magnetic field acting on its spin. The SOI plays an important role in the field of spintronics since it is in most cases responsible for spin rotation and decoherence effects. Recently an increased interest has been focused on a consequence of the SOI, namely a spatial spin accumulation in a two-dimensional system in the absence of a magnetic field, known as the spin Hall effect.^{1,2,3,4,5,6,7,8,9,11} Another SOI-induced phenomenon of current interest is the *Zitterbewegung* of electrons in semiconductors,^{12,13,14} in analogy with the oscillating behavior of a free relativistic electron due to interference between its positive- and negative-energy state components. The previous theoretical works were focused on two-dimensional systems or quasi-one-dimensional systems with injection in the lowest subband only. However, in a realistic experimental setup the Fermi energy and width of the sample are typically set at values for which the electron transport is in the multi-subband regime. It is known that the SOI will induce interaction between these subbands as well as the spin states.^{15,16,17} These interactions will bring an initially prepared spin state into a quantum-coherent spin-mixed state and can give rise to complicated spin-dependent electron transport phenomena. To capture all the physics of the problem an exact multi-subband treatment is hence necessary.

In this paper we will study the intrinsic spin-Hall effect and Zitterbewegung in a multi-channel electron waveguide system in the absence of an external magnetic field. We will show that the Zitterbewegung and the intrinsic spin Hall effect is essentially the same phenomenon. In the multi-channel regime, a remarkable reversal of the spin Hall effect between different channels is found which can not be explained by a simple heuristic force operator consideration previously adopted in the literature. We will further show that for wide waveguides, supporting multiple open subbands, spin accumulation patterns are formed inside the waveguide in addition to the usual edge spin accumulations in the intrinsic spin Hall effect. These patterns, formed as a coherent state in the waveguide,

are found to be directly proportional to the number of conducting channels in the leads.

To study the problem we consider a two-dimensional electron gas (2DEG) formed in the x - y plane of a semiconductor heterostructure. The 2DEG is restricted to a waveguide by a hard-wall confinement potential $U_c(y)$ in the transverse y -direction, $U_c(y) = 0$ for $y \in [-w/2, w/2]$ and ∞ otherwise, with w being the width of the waveguide. The structure is subjected to a homogenous electrical field along the unit vector ξ giving rise to Rashba spin-orbital interaction of strength α . For crystal structures lacking inversion symmetry, there will in addition be a Dresselhaus SOI contribution characterized by the strength β . Such inversion asymmetry is found in, e.g., the zinc-blende crystals of the III-V materials. The waveguide is connected with two perfect semi-infinite leads of vanishing SOI contributions from which the electrons are injected at one end and transported coherently in the longitudinal x -direction. The model Hamiltonian describing such a system under the effective mass approximation has the form

$$H = \frac{\mathbf{p}^2}{2m^*} + U_c(y) + \frac{1}{2\hbar} \left[\alpha(\mathbf{r}) \boldsymbol{\sigma} \cdot (\mathbf{p} \times \boldsymbol{\xi}) + \beta(\mathbf{r}) (\sigma_x p_x - \sigma_y p_y) + H.c. \right], \quad (1)$$

where \mathbf{p} is the momentum operator, m^* the electron effective mass taken to be $m^* = 0.042 m_e$, corresponding to an InGaAs quantum-well system, and $\boldsymbol{\sigma}$ the vector of the spin operators. The inclusion of SOI will break the reflection invariance of the system in the transverse direction, i.e., $[R_y, H] \neq 0$. However, for a symmetric confining potential the system is invariant under operation of $\sigma_y R_y$, i.e., $[\sigma_y R_y, H] = 0$. This symmetry has an important implication: for a spin-unpolarized injection electron beam the spin-up electron probability distribution in the system is exactly the mirror image of the spin-down electron probability distribution with respect to the transverse reflection R_y . Thus, if an accumulation of spin occurs on one side of the waveguide, the same amount of accumulation of the opposite spin will occur on the other side of the waveguide. Since an unpolarized

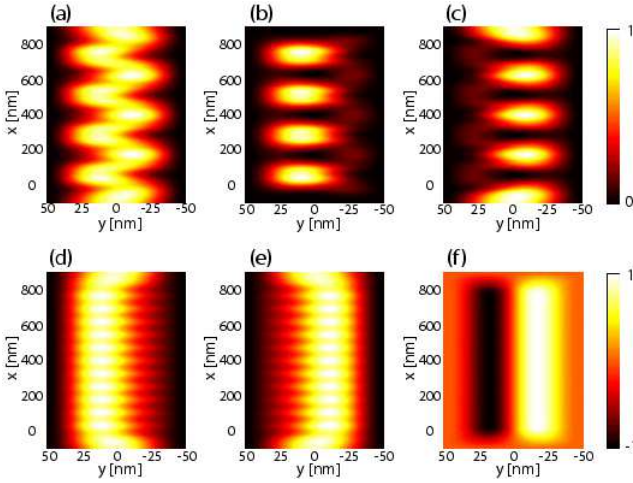


FIG. 1: (a)-(c) Normalized probability distribution for an electron injected in a spin-up state. (a) Total probability distribution, ρ_1^\uparrow . (b) Spin-down projection, $\rho_1^{\downarrow\uparrow}$. (c) Spin-up projection, $\rho_1^{\uparrow\uparrow}$. (d)-(f) Normalized probability distribution for an unpolarized electron. (d) Spin-down projection, $\rho_1^{\downarrow\uparrow} + \rho_1^{\downarrow\downarrow}$. (e) Spin-up projection, $\rho_1^{\uparrow\uparrow} + \rho_1^{\uparrow\downarrow}$. (f) Polarization probability distribution, $\rho_1^{\uparrow\uparrow} + \rho_1^{\uparrow\downarrow} - \rho_1^{\downarrow\uparrow} - \rho_1^{\downarrow\downarrow}$. In all figures $w = 100$ nm and $\alpha = 3 \times 10^{-11}$ eVm for $x \in [0, 800]$ nm and decreased adiabatically down to zero for $x \in [-100, 0] \cup (800, 900]$ nm. The upper scale bar shows the measure for plots (a)–(e), while the lower scale bar shows the measure for plot (f).

injection electron beam is an incoherent mixed spin-state, this symmetry asserts that all information of the probability distribution, regardless of the injection condition, is contained in the probability distribution of a polarized injection beam. One needs only consider one polarization direction of the injection since the result from the other injection condition follows from the symmetry requirements.

The probability distribution, $\rho^\gamma(x, y)$, for electrons injected from a lead, say the left lead, in a pure spin- γ state can be obtained from

$$\rho^\gamma(x, y) = \sum_{q\sigma} \rho_q^{\sigma\gamma}(x, y) \sim \sum_{\sigma} \sum_{\{q|k_q \in \mathbb{R}\}} \frac{|\langle \chi(\sigma) | \Psi_q^\gamma(x, y) \rangle|^2}{k_q}, \quad (2)$$

where $\Psi_q^\gamma(x, y)$ is the wavefunction for an electron injected from the left lead in the q th subband with spin $\gamma = \uparrow$ or \downarrow , $|\chi(\gamma = \uparrow)\rangle = (1, 0)^T$ and $|\chi(\gamma = \downarrow)\rangle = (0, 1)^T$ are the two spin states with the spin quantization axis along the electric field direction, $k_q = [2m * (E_F - E_q)/\hbar^2]^{1/2}$ with E_F being the Fermi energy and E_q the q th subband energy in the injection lead, and $\rho^{\sigma\gamma}(x, y)$ is the projected spin- σ probability distribution. In the present study, the wave function Ψ_q^γ is calculated by employing an exact, spin-dependent, multi-mode scattering matrix technique.¹⁷

Consider now the case when only the Rashba SOI is present, i.e., $\beta = 0$ and $\alpha \neq 0$. Since $[\sigma_i, H] \neq 0$, $\forall i$, an

electron initially prepared in a pure spin-state in the lead will evolve into a quantum-coherent mixed-spin state as it travels through the waveguide of finite SOI. This coherent spin evolution will give rise to spin-waves along the waveguide. To visualize these properties, we calculate the electron probability distributions in the waveguide, with the electric field, ξ , set along the z -direction. We start by assuming the width of the waveguide $w = 100$ nm and the Fermi energy $\epsilon_F = 2$ meV corresponding to the case that one channel is open in the leads. The SOI strength is taken to be $\alpha = 3 \times 10^{-11}$ eVm in the region with the full strength of the Rashba SOI, defined in $x \in [0, 800]$ nm, and decreased adiabatically down to zero in the transition regions of the entrance and exit defined in $x \in [-100, 0]$ and $x \in [800, 900]$ nm. Figure 1(a) shows the calculated total (charge) probability distribution $\rho^\uparrow = \rho^{\uparrow\uparrow} + \rho^{\uparrow\downarrow}$ for electrons injected in a pure spin-up state. It is seen that the electron exhibits a transversely oscillating probability distribution along the waveguide. This is Zitterbewegung arising from interference between the two spin branches of the Hamiltonian. By considering the spin-up [Fig 1(b)] and the spin-down [Fig 1(c)] projections separately, clear spin-wave patterns are found in the form of spatially separated localized islands of high probability density. The two spin-dependent probability distribution components, $\rho^{\uparrow\downarrow}$ and $\rho^{\downarrow\uparrow}$, corresponding to a spin-down injection condition can be obtained from mirror reflection of the corresponding results shown in Figs. 1(a)–1((c)) as required by $[\sigma_y R_y, H] = 0$. It is evident that the spin-up and spin-down electron wave-function components are localized in different sides of the waveguide. This accumulation of different spins along opposite edges of the waveguide is a fundamental property of the spin-Hall effect observed recently. The spin projected electron probability distributions for an unpolarized injection source are shown in Fig. 1(d) and 1(e). Due to the symmetry of the system under the operation of $\sigma_y R_y$, the total distribution will be symmetrical in the transverse direction, and the spin-up, Fig. 1(d), [spin-down, Fig. 1(e)] probability distribution is the mirror image of the corresponding spin-down [spin-up] probability distribution. Hence no spin-polarization will be detected in the measured two-terminal conductance. This was rigorously shown, in Refs. 19 and 20, to always hold, independent on the details of the conductor, when only one channel is open for conduction in the leads. Accumulations of electron spins with opposite polarizations at the opposite edges of a wide conductor have recently been experimentally observed.^{6,7,8} What is measured in such experiments is the net spin density at a given position in the sample for a spin-unpolarized electron injection source, which can be quantified by the spin-polarized probability distribution, $\rho_{pol} = \rho^{\uparrow\uparrow} + \rho^{\uparrow\downarrow} - \rho^{\downarrow\uparrow} - \rho^{\downarrow\downarrow}$, shown in Fig. 1(f). Clear spin separation along the edges of the waveguide is found which is the signature of the spin-Hall effect. One can see that the spin-Hall effect and the Zitterbewegung is essentially the same phenomenon since one follows from the other depending on if only one or both spin states

are considered to be injected and whether the spin accumulation or the charge accumulation is measured. In other words, the results of Figs. 1(a),(d),(e) and (f) can be constructed from Figs. 1(b) and (c) and their mirror images.

When the Fermi energy is increased more conducting channels are opened for conduction in the leads. Figure 2 shows the probability distributions for the Fermi energy $\epsilon_F = 12$ meV corresponding to 3 open channels in the leads. In Fig. 2(a)-(f) the spin projected probability distributions for a spin-up electron injected separately in the three channels are shown. The probability distribution for polarized injection in the lowest channel, $\rho_1^{\uparrow\uparrow}$ and $\rho_1^{\downarrow\uparrow}$, shown in Figs. 2(a) and (b) exhibits qualitatively similar Zitterbewegung and spin-Hall patterns as was found in the single channel system in Fig. 1. However, a remarkable reversal of the spin parity is found where the spin-up(down) projected probability density is localized along the left(right) edge of the waveguide. This is also true for the probability distribution corresponding to injection in the second channel, $\rho_2^{\uparrow\uparrow}$ and $\rho_2^{\downarrow\uparrow}$, shown in Figs. 2(c) and (d). Only the probability distribution corresponding to injection in the highest subband, $\rho_3^{\uparrow\uparrow}$ and $\rho_3^{\downarrow\uparrow}$, Figs. 2(e) and (f), exhibits the spin parity found in the single-channel system. We note that this phenomenon can not be explained by the force operator derived from the Hamiltonian as considered in ,e.g., Ref 10 and implies that such a heuristic approach fails for more complicated systems such as multi-channel transport. Indeed, for equilibrium systems considered here, no resulting force is present and the observed Zitterbewegung and spin-Hall effect are merely coherent, non-dynamical states. In light of these findings, one may ask if the Zitterbewegung and spin-Hall effect can still be observed in the multi-channel system. To answer this we show in Fig. 2(g) the total probability distribution, ρ^{\uparrow} , for a spin-polarized simultaneous injection in the three open channels. It is seen that Zitterbewegung oscillation is still found along the waveguide, albeit more complicated as compared to the single-channel system. The calculated spin polarization distribution, ρ_{pol} , shown in Fig. 2(h) exhibits regular spin density patterns. Strong spin polarization with opposite sign is found at the two edges of the waveguide, as observed in recent experiments. However, spin accumulations, with a pattern of alternative spin-polarization stripes, also occurs inside the waveguide. The number of stripes for each spin-polarization direction is equal to the number of the open channels in the waveguide. It is important to note that this internal structure is formed as a coherent state in the waveguide in the equilibrium regime and not due to diffusion between the lateral edges. Experimental observation of the internal spin-polarization structure is certainly an interesting but challenging issue, because it requires a spin detection setup with a high spatial resolution (about 50 nm or better for the system discussed in this work).

For a wide conductor, a large number of channels are typically open for conductance and the inter-subband

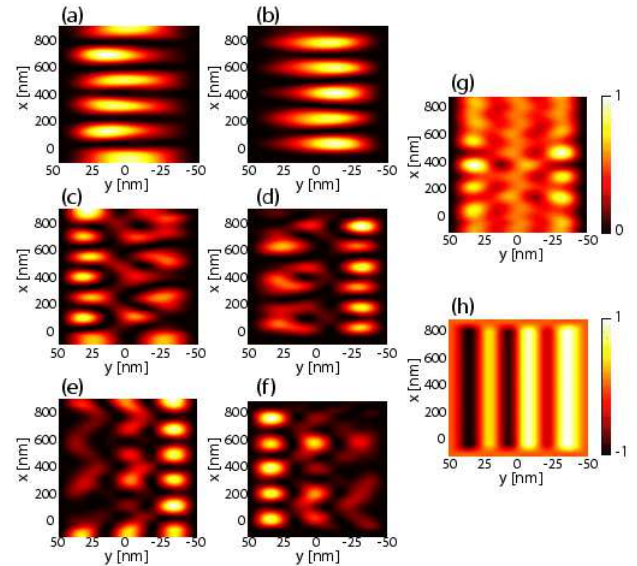


FIG. 2: (a)-(f) Normalized spin projected probability distribution for a spin-up electron injected separately in the three open channels of the leads. (a) $\rho_1^{\uparrow\uparrow}$. (b) $\rho_1^{\downarrow\uparrow}$. (c) $\rho_2^{\uparrow\uparrow}$. (d) $\rho_2^{\downarrow\uparrow}$. (e) $\rho_3^{\uparrow\uparrow}$. (f) $\rho_3^{\downarrow\uparrow}$. (g) Normalized total probability distribution for a spin-up electron injected simultaneously in the three propagating modes of the leads, ρ^{\uparrow} . (h) Normalized polarization probability distribution for an unpolarized electron injected simultaneously in the three open channels of the leads, ρ_{pol} . In all figures $w = 100$ nm, $\epsilon_F = 12$ meV and $\alpha = 3 \times 10^{-11}$ eVm for $x \in [0, 800]$ nm and decreased adiabatically down to zero for $x \in [-100, 0] \cup (800, 900]$ nm. The upper scale bar shows the measure for plots (a)-(g), while the lower scale bar shows the measure for plot (h).

mixing induced by the SOI can produce a complicated pattern in the probability distribution. In Fig. 3 we show ρ_{pol} in two wide waveguides of width $w = 370$ nm and $w = 1 \mu\text{m}$ corresponding to 5 and 14 open channels respectively at strong and weak SOI strength. The distribution is symmetric with respect to $\sigma_y R_y$ and for a weak SOI strength, Figs 3(a) and (c), the same structural pattern as observed in the narrower waveguides is found. For strong SOI strength, Figs. 3(b) and (d), lateral spin accumulation can be observed along two transversely displaced lines of opposite spin with the inner line being what would be expected from the narrow waveguide data. This strong interaction, multi-channel system is far more complicated than the single-channel case. However, what is significant is the observation of spatial spin accumulations even under these circumstances.

Since the Rashba and the Dresselhaus terms in the Hamiltonian are related through a similarity transform, all the presented results hold for the case when only the Dresselhaus SOI is present, i.e. $\alpha = 0$, $\beta \neq 0$ with the substitution $x \rightarrow -x$ and $y \rightarrow -y$. For $\alpha = \pm\beta$ the spin-dependent part of the Hamiltonian takes the form

$$H_{\pm}^s = \frac{\alpha}{\hbar} (p_y \pm p_x) \boldsymbol{\sigma} \cdot (\mathbf{e}_x \mp \mathbf{e}_y). \quad (3)$$

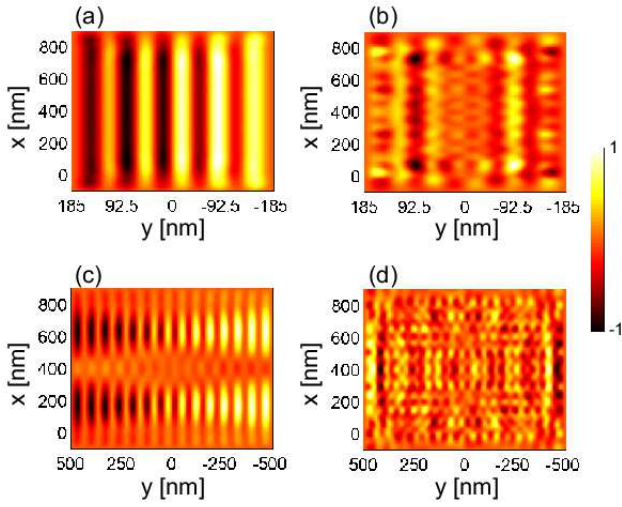


FIG. 3: Normalized polarization probability distribution, ρ_{pol} , for an electron injected in an unpolarized state. (a) $w = 370$ nm, $\alpha = 1 \times 10^{-11}$ eVm (b) $w = 370$ nm, $\alpha = 3 \times 10^{-11}$ eVm (c) $w = 1000$ nm, $\alpha = 0.1 \times 10^{-11}$ eVm (d) $w = 1000$ nm, $\alpha = 3 \times 10^{-11}$. Spin-orbit strength α is finite for $x \in [0, 800]$ nm and decreased adiabatically down to zero for $x \in [-100, 0] \cup (800, 900]$ nm.

The SOI induced effective magnetic field direction is in this case independent of the momentum. This means that

a well-defined quantization axis can be found throughout the SOI region and spin is therefore a conserved quantity. In Ref. 21 it was shown that in III-V systems the Rashba and Dresselhaus SOI can be of comparable strengths. This would imply that no Zitterbewegung¹² nor spin-Hall effect should occur in this situation.

In conclusion, we have calculated spin resolved electron probability distributions and a Zitterbewegung pattern was observed for a narrow waveguide with injection in one and three channels. By analyzing the spin projected probability distributions for separate injection in the individual channels, a remarkable spin parity change was revealed between the different channels which can not be explained by a heuristic force operator consideration. For an electron injected in an unpolarized state, spin accumulation will appear along the edges of the wave-guide resulting in the spin-Hall effect. We also calculated the spin polarized probability distribution for a wide waveguide with multiple open channels and spin accumulations along the lateral edges were observed as well as internal spin accumulation patterns of alternating spin-polarization. These patterns are formed as coherent states in the equilibrium regime. To measure these patterns a spatial resolution of ~ 50 nm or better is needed. We have also shown that the Zitterbewegung and the spin-Hall effect are stemming from the same mechanism and is only differing in the injection and measuring conditions.

* Electronic address: Patrik.Brusheim@ftf.lth.se
 † Corresponding author; Electronic address: Hongqi.Xu@ftf.lth.se
¹ J. E. Hirsch, Phys. Rev. Lett. **83**, 1834 (1999).
² S. Zhang, Phys. Rev. Lett. **85**, 393 (2000).
³ L. Sheng, D. N. Sheng, and C. S. Ting, Phys. Rev. Lett. **94**, 016602 (2005).
⁴ E. M. Hankiewicz, L. W. Molenkamp, T. Jungwirth, and J. Sinova, Phys. Rev. B **70**, 241301(R) (2004).
⁵ M. I. D'yakonov and V. I. Perel, JETP Lett. **13**, 467 (1971).
⁶ Y. K. Kato, R.C. Myers, A. C. Gossard, and D. D. Awschalom, Science **306**, 1910 (2004).
⁷ V. Sih, R. C. Myers, Y. K. Kato, W. H. Lau, A. C. Gossard, and D. D. Awschalom, Nature Phys. **1**, 31 (2005).
⁸ J. Wunderlich, B. Kaestner, J. Sinova, and T. Jungwirth, Phys. Rev. Lett **94**, 047204 (2005).
⁹ B. K. Nikolić, S. Souma, L. P. Zárbo, and J. Sinova, Phys. Rev. Lett. **95**, 046601 (2005); B. K. Nikolić, L. P. Zárbo, and S. Souma, Phys. Rev. B **72**, 075361 (2005)
¹⁰ B. K. Nikolić, L. P. Zárbo, and S. Welack, Phys. Rev. B. **72**, 075335 (2005).

¹¹ J. Sinova, D. Culcer, Q. Niu, N. A. Sinitsyn, T. Jungwirth, and A. H. MacDonald, Phys. Rev. Lett. **92**, 126603 (2004).
¹² J. Sclieemann, D. Loss, and R. M. Westervelt, Phys. Rev. Lett. **94**, 206801 (2005).
¹³ M. Lee and C. Bruder, Phys. Rev. B **72**, 045353 (2005).
¹⁴ Z. F. Jiang, R. D. Li, S-C. Zhang, and W. M. Liu, Phys. Rev. B **72** 045201 (2005).
¹⁵ F. Mireles and G. Krirczenow, Phys. Rev. B **64**, 024426 (2001).
¹⁶ X. F. Wang, Phys. Rev. B **69**, 035302 (2004).
¹⁷ Lebo Zhang, P. Brusheim, and H. Q. Xu, Phys. Rev. B **72**, 045347 (2005).
¹⁸ D. Yuk Kei Ko and J. C. Inkson, Phys. Rev. B **38**, 9945 (1988).
¹⁹ F. Zhai and H. Q. Xu, Phys. Rev. Lett. **94**, 246601 (2005).
²⁰ E. N. Bulgakov and A. F. Sadreev, Phys. Rev. B **66**, 075331 (2002).
²¹ J. B. Miller, D. M. Zumbühl, C. M. Marcus, Y. B. Lyanda-Geller, D. Goldhaber-Gordon, K. Campman, and A. C. Gossard, Phys. Rev. Lett. **90**, 076807 (2003).